Applied Surface Science 722 (2026) 165552

Contents lists available at ScienceDirect

Applied Surface Science

journal homepage: www.elsevier.com/locate/apsusc

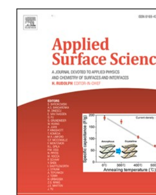

Full Length Article

Microscopic control of SiGe/high-κ oxide gate stack for p-MOSFET hole qubits

Ibrahim B. Adetunji [a,b], Francesco Tavanti [a,c,*], Alessandra Catellani [a], Arrigo Calzolari [a]

[a] CNR-NANO Istituto Nanoscienze, Centro S3, Modena I-41125, Italy
[b] Bells University of Technology, Physical Sciences Department, Ota, Ogun State, Nigeria
[c] Department of Chemical Sciences, University of Padova, via Marzolo 1, Padova 35100, Italy

ARTICLE INFO

Keywords:
Oxides interface
Ab-initio
Molecular dynamics
Amorphous

ABSTRACT

The formation of GeO_x and $HfGeO_x$ by-products, and the Ge diffusion at the interface between SiGe active layer and high-κ amorphous gate oxide (a-HfO_2) are major issues that affect the mobility of SiGe channels in p-type metal–oxide–semiconductor field-effect transistors (MOSFETs). Experimental evidence suggests that the inclusion of multiple interlayers and Nitrogen incorporation may reduce these interface defects and prevent the formation of detrimental traps at the SiGe/oxide contacts. In this work, we address the problem by combining density functional theory and classical molecular dynamics simulations. Our results reveal that the introduction of an ultrathin a-SiO_2/a-SiON bilayer between SiGe and a-HfO_2 is an efficient solution to eliminate the mixed oxides formation, preventing the diffusion of germanium into the gate oxide and improving the p-MOSFET efficiency.

1. Introduction

The potential of silicon-based charge-spin quantum-dot qubits as material for commercial complementary metal oxide semiconductor (CMOS) technology has generated a lot of interest due to their record coherence times and fidelity [1–4]. Despite of these characteristics, their operation has been limited to temperatures below 100 mK because of the low confinement and coupling energies [5,6]. Yet, getting qubit with higher confinement, higher coupling energies, and with spin resonance in the upper mm-wave region will give room for higher temperature operation. On the technological side, MOSFETs are the building blocks of modern electronic devices [7–9]. Thus, being able to realize stable qubits by exploiting the MOSFET technology would take advantage of the huge know-how in the field with an evident technological gain. Many materials such as Si-channel n-MOSFETs (electron-spin qubit) and SiGe-channel p-MOSFETs (hole-spin qubit) [10] are now being investigated for the realization of quantum-dot qubits with higher temperature and fidelity for quantum computing. In this case, the control and the stability of the resulting qubits rely on the control and the stability of the underlying MOSFETs device.

The size reduction and scaling of MOSFETs have contributed to the increased transistor density, improved performance and decreased power consumption in electronic devices [11–14]. However, these remarkable gains are faced with problems such as low mobility of substrates, or metal gate and high-κ dielectric integration [15–17]. Many efforts have been directed towards searching for: **i.** semiconductor channels with mobility higher than crystalline Si [18–24], for example strained silicon (sSi), $Si_{1-x}Ge_x$ (SiGe), Ge and group III-V semiconductors [22,25–27]; **ii.** new gate materials with high-κ dielectric alternative to the traditional amorphous a-SiO_2 in order to reduce gate leakage, such as a-HfO_2, a-ZrO_2, Al_2O_3, Y_2O_3 and La_2O_3 [15,28].

Among these materials, SiGe and amorphous HfO_2 (a-HfO_2) are been considered the materials of choice for the fabrication of p-MOSFETs (Fig. 1a) [29–34]. SiGe shows a high carrier mobility that can be fine-tuned by controlling the Ge content; while a-HfO_2 reduces the gate leakage with respect to fixed equivalent oxide thickness. Furthermore, a-HfO_2 has good thermodynamic and chemical stability, reasonable band offset and lack of dislocations and grain boundaries, which are prominent in the crystalline oxide gates [35–37]. The major concern in the implementation of these two materials into MOSFETs is the nature and quality of their inherent interface. The presence of interface defects is responsible for degradation which eventually affects the device performances.

Two main aspects are particularly critical: i. the formation of Si-O dangling bonds at the interface, which are responsible for trapping electronic states in the channel band- gap region [38–44]; ii. the

* Corresponding author at: Department of Chemical Sciences, University of Padova, via Marzolo 1, Padova 35100, Italy.

https://doi.org/10.1016/j.apsusc.2025.165552
Received 14 July 2025; Received in revised form 11 December 2025; Accepted 11 December 2025
Available online 12 December 2025
0169-4332/© 2025 The Author(s). Published by Elsevier B.V. This is an open access article under the CC BY-NC-ND license (http://creativecommons.org/licenses/by-nc-nd/4.0/).

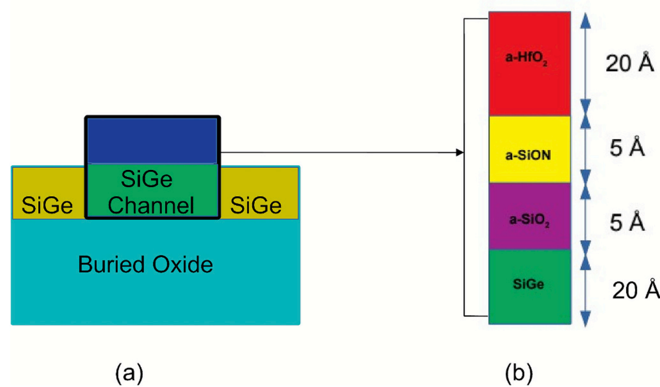

Fig. 1. Simplified cross-sectional scheme of SiGe p-MOSFET quantum dot.

diffusion of Ge atoms into the oxide layer and the formation of under-coordinated GeO_x complexes that nucleate the growth of GeO_2 impurities [45–49].

The formation of SiO_x dangling bonds can be reduced by including a subnanometer layer of oxides such as SiO_2 [37,50] or Al_2O_3 [51], while selective oxygen scavenging [40,52] and passivation with nitrides and sulfur [53–58] are useful to decrease the amount of Ge concentration [43]. However, these solutions are not sufficient to prevent Ge to diffuse through the oxide surface, resulting into degrading defect states. This drawback can be mitigated using multiple interlayer (IL) insertion within the SiGe/a-HfO_2 interface.

In this study, we investigated the SiGe/a-SiO_2/a-SiON/HfO_2 gate stack, following the experimental prescriptions proposed by S. Krishnan and coworkers [59,60]. The inclusion of the two ILs improves the stability of the overall system, by reducing the formation of both SiO_x and GeO_x dangling bonds. Albeit this model structure has been adopted *de facto* by several fabrication factories, the origin of this behavior is still unclear. Here, by using a multi- scale/multi-physics approach based on classical molecular dynamics and density functional theory (DFT), we provide a microscopic understanding of this multilayer channel-gate stack. This opens the way to the realization of stable and controllable SiGe-channel p-MOSFETs that could be used for the production of quantum-dot qubits with high temperature and fidelity.

2. Methods

Structural and electronic ground-state simulations have been carried out through first principles approaches based on density functional theory, as implemented in the Quantum Espresso(QE) package [61–63]. In the treatment of the exchange–correlation potential, we used PBE generalized gradient approximation (GGA) [64]. Atomic potentials were described by ultrasoft pseudopotentials of the Vanderbilt's type [65]. Single particle wavefunctions and charge were expanded on a plane wave basis with kinetic energy cutoff of 25 Ry and 250 Ry respectively that give a good compromise between accuracy and computational cost for both layer and interface systems. In the case of bulk HfO_2 only, the cutoff was chosen to be 50 Ry to take have a higher resolution in the possible localized states. Brillouin-zone integration was performed using Γ-point during the atomic relaxation, and with a uniform $(2 \times 2 \times 1)$ Monkhorst-Pack k-points mesh for the evaluation of the electronic structure.

Underestimation of the band gap, typical of standard DFT-GGA functionals, has been corrected by including a Hubbard-like potential, within the DFT + U frameworks along the lines described, e.g., in Ref. [66]. The optimized values for chemical species have been obtained for each isolated compound (i.e. SiGe, SiO_2, SiON, and HfO_2) by using the pseudohybrid Hubbard Density Functional approach (namely ACBN0) [67], implemented in the AFLOWπ infrastructure code [68]. The effects of the ACBN0 approach on the structural, electronic and vibrational properties of inorganic semiconductors have been largely tested in previous reports (see e.g. Refs. [69,70]).

The semiconductor channel is modeled through a periodic supercell including a $Si_{0.75}Ge_{0.25}$(001) surface, accordingly to experimental works and commonly fabricated devices and previous works [37,71], with a (2×2) lateral periodicity of dimension (11.15×11.15) Å^2 and 11.15 Å of thickness, obtained through geometry optimization of the $(2 \times 2 \times 2)$ cubic supercell. A 15Å-thick layer of vacuum was added to prevent interactions between periodically repeated slab replicas. The bottom layer was passivated with Hydrogen atoms. Hereafter, if not explicitly stated, we will refer $Si_{0.75}Ge_{0.25}$ simply as SiGe.

In order to simulate the SiGe/oxide stacks, we considered the direct SiGe/a-HfO_2 interface and three multilayers with increasing complexity, as presented in Fig. 1(b): (i) SiGe/a-SiO_2, (ii) SiGe/a-SiO_2/a-SiON, and (iii) SiGe/a-SiO_2/a-SiON/a-HfO_2.

The initial structure of the single amorphous oxides SiO_2, SiON and HfO_2, have been obtained from classical molecular dynamics simulations. The three amorphous materials have been modeled in bulk-like configurations having the same lateral periodicity of the SiGe substrate (i.e. 11.154 Å), and different thicknesses, as proposed in the experimental systems [59]: 5.0 Å for both SiO_2 and SiON, 20.0 Å for HfO_2. The respective crystal structures have been melted to a temperature of 3000 K for 10 ns in order to have a complete liquid phase ensuring the loss of the initial memory of the crystalline system. Then, each system has been cooled down to the temperature of 300 K with a cooling rate of 10 K/ps, which ensures the correct formation of the amorphous/glass phase while maintaining a quite low computational effort [72]. After the system reached the 300 K temperature, a production run of 20 ns in the NVT ensemble has been performed at constant temperature of 300 K using the Nose-Hoover thermostat with a coupling time of 1 ps and with a timestep of 2 fs. All classical MD simulations have been performed using the GULP package [73]. For each system, we employed different force fields that were able to reproduce the main structural features of the single materials: for SiO_2 the parameters were obtained from the work of Pedone et al. [74], explicitly developed for glassy dioxides; for SiON the Reax force field from Van Duin et al. [75] has been used; and for the HfO_2 parameters were obtained from the work of Broglia et al. [76] that accurately describe lattice parameters and bond lengths. The radial distribution function, g(r), (see *Supplementary Materials Fig. S1*) has been computed on the last 5 ns of the production run using the VMD package [77]. A representative snapshot of each oxide bulk has been assumed as initial structure for the DFT total-energy-and-forces optimization of the corresponding 2D layer, obtained by including in the simulation cell a vacuum space in the direction perpendicular to the surface. The final DFT configuration for each layer (SiO_2, SiON and HfO_2) was used to compose the stacks. By construction, all amorphous layers were generated in a simulation cell having the same lateral periodicity of SiGe(001) and then relaxed at the DFT layers. For the preparation of the interface structures, we sequentially stacked the relaxed oxide layers on top of the SiGe slab. Thus, the SiGe/a-SiO_2 interface is obtained by setting the a-SiO_2 layer on the SiGe (001) surface and then relaxed with DFT. Then, the SiON layer was added on the previous relaxed SiGe/a-SiO_2 interface; the ternary system has been further relaxed at the DFT level. Lastly, the HfO_2 was stacked on the ternary system obtaining the SiGe/a-SiO_2/a-SiON/a-HfO_2 multilayer that has been also optimized at the DFT level. Each IL has been manually placed over the previous structure avoiding superimposition of atoms by maintaining an initial average distance between interface atoms of $\sim$2 Å, which is of the order of the average distance between pairs involved in the interfaces (e.g. Si-O, Si-Ge, etc). Atomic bonds at the interface are optimized during the relaxation processes. Notably, since oxides are amorphous, they can easily accommodate small deviations in atomic positions without introducing long-range elastic strain. In a similar way, the binary SiGe/HfO_2 interface, i.e. without ILs, has been also simulated for comparison, by combining the two composing slabs.

All the structural DFT relaxations were performed using QE. All unrelaxed and relaxed atomic structures are collected in the *Supplementary Materials Figs. S2(a–d)*. This procedure to build multi-layer stacks has been already employed in previous work, where crystalline surfaces have been capped with amorphous materials for electronic applications and showing very good agreement with experimental results on devices [78].

3. Results and discussion

3.1. Composing layers

We first considered the SiGe surface and the single oxide layers, separately. Structural relaxation plays a key role in the realization of stable amorphous oxides, because of the presence of local-order structures and non-stoichiometric defects (e.g. over- and under- coordinated atoms). Bond lengths of each material are reported in Table 1 and compared with previous results obtained by Neutron diffraction, EXAFS, and ab initio molecular dynamics simulations. All values from both MD and DFT are close to each other and in good agreement with previously published results. In the case of SiON, the N-N first peak of g(r) at 1.11 Å is very narrow and followed by a broader peak at 2.90 Å, in agreement with experimental work [79]. Major structural rearrangements occur at SiGe surface where Si and Ge atoms from rows of buckled dimers along the [1 1 0] direction, see *Supplementary Materials Fig. S2(a)*. The resulting Si-Si, Ge-Ge and Si-Ge bond lengths from g(r) (2.42 Å, 2.49 Å, 2.44 Å, respectively) are in agreement with the reported data [80–82]. Similarly, a-HfO_2 and a-SiO_2 structures undergo strong atomic rearrangement at surface, as presented in *Supplementary Materials Figs. S2(b and d)*. The Si-O and Hf-O bond lengths before and after relaxations in both structures are 1.65(1.63) and 2.19(2.07) Å respectively, in agreement with available data [83–85]. In the case of a-SiON, a very pronounced redistribution of Si, O and N atoms occurred after DFT relaxation (*Supplementary Materials Fig. S2(c)*). This is most probably due to the Force Field employed in MD simulation that is not specific for SiON alloys. In particular, we observed the formation of 2N-N dimers and the clustering of Si and O atoms. The Si-O, Si-N and N-N bond lengths before and after relaxation are: 1.55(1.65), 1.95(1.71) and 1.25 (1.25) Å respectively. The optimized DFT values are in agreement with available data [86].

The density of states (DOS) plots of SiGe and of the three considered oxides are shown in Fig. 2(a–d), the zero energy reference is set to the Fermi level (E_F) of each system. Electronic structures were calculated

Table 1
The bond lengths expressed in Å for each pair for the three amorphous systems obtained by classical Molecular Dynamics (MD) and by DFT calculations (DFT).

System	Bond (Å)	This work (MD)	This work (DFZ)	Exptl. And Comp. results
SiO_2	Si–O	1.65	1.63	1.61[a]
	Si–Si	3.07	3.05	3.07[a]
	O–O	2.63	2.65	2.63[a]
SiON	Si–O	1.55	1.65	1.61[a]
	Si–Si	3.07	3.00	3.06[b]
	O–O	2.50	2.65	2.60[b]
	Si–N	1.95	1.71	1.73[b]
	O–N	2.90	2.75	
	N–N	1.25/2.90	1.25	2.97[b]
HfO_2	Hf–O	2.08	2.07	2.08/2.11[c]
	Hf–Hf	3.53	3.32/3.80	3.32/3.39[c]
	O–O	2.70	2.65	2.55/2.69[c]

[a] Ref. [87] and [88].
[b] Ref. [79].
[c] Ref. [76] and [89].

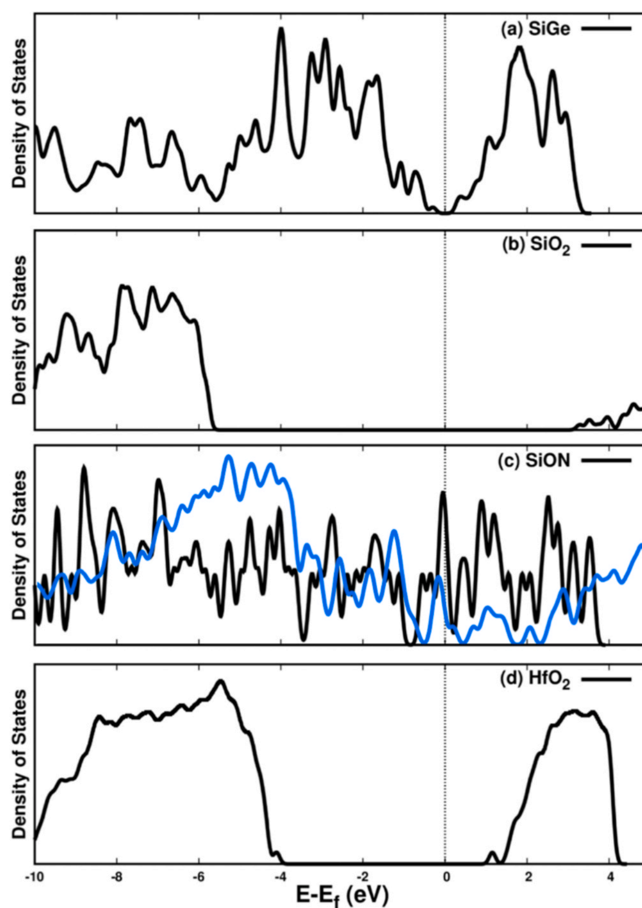

Fig. 2. Density of states (DOS) plots for (a) SiGe(001), (b) a-SiO_2, (c) a-$SiON_2$, and (d) a-HfO_2 isolated surfaces. Vertical dashed lines mark the Fermi energy (E_F) of each system. In panel c) the black line represents the 42 atoms system and the blue line the 126 atoms system.

within the DFT + U framework (see Method). SiGe, a-SiO_2 and a-HfO_2 exhibit the expected semiconductor character, with a calculated energy bandgap of 0.58 eV, 9.05 eV and 5.24 eV respectively, in excellent agreement with previously reported data [35,90]. No defect states are observed in the gap, except for a small shallow state appearing close to the conduction region for a-HfO_2. On the contrary, a-SiON displays a conductor-like behavior, with no-recognizable band gap (Fig. 2(c)) in contrast with the 2–5.5 eV gaps reported for crystalline and stoichiometric amorphous Si_2N_2O [91]. This is due to the non-stoichiometric composition and high defect density of the simulated layer, arising from the melt-quench procedure, and due to the small thickness of the film that favors the formation of trap states in the gap [92]. In particular, the model layer contains undercoordinated Si and N atoms, Si–Si bonds, and oxygen vacancies, each of them generates localized states which fill and reduce the nominal mobility gap. This result is consistent with previous reports of effective band gap narrowing in SiON for O/N-deficient compositions or high concentrations of coordination defects [91,92]. The high number of dangling bonds in SiON thin film is mainly given by O and N atoms that are not fully coordinated, especially those on the surface. However, the number of O-dangling bonds drastically reduces when the SiON stack is deposited on the SiGe-SiO_2 interface with fewer N-dangling bonds that still persist due to the presence of surface atoms exposed to vacuum. Yes, this is an intermediate configuration during the growth process. Indeed, when HfO_2 also cover the topo of the stack, these defect states fully disappear, as reported in Fig. S3. This confirms that the presence of frustrate bonds (and corresponding defect states in the DOS) in the isolated films of in the intermediate

structures is not an issue for the final multilayer. Therefore, the absence of a net gap in our model is a feature of the specific ultra-thin, disordered, defect-rich SiON layer structure generated here, while it is not representative of ideal stoichiometric Si_2N_2O bulk, which has a well-established semiconducting behavior. To confirm this trend, we built for comparison a thicker SiON layer (12.311 Å) composed of 126 atoms in its amorphous state phase and performed electronic states calculation using the same set of parameters of the other runs. By computing the DOS (blue line in Fig. 2c), we observe a band gap of approximately 6 eV with several trap states within the gap, confirming that lowering the SiON thickness results in an increase in the defect states that close the real band gap.

The electronic states across the Fermi level stem mostly from the 2*p* lone pairs of nitrogen, as previously reported in Ref. [92]. However, the comparison between the single-particle orbitals of a-SiO_2 and a- SiON indicates that an evenly amount of O atoms also contributes to the metal-like feature of a-SiON.

3.2. Multilayer stacks

Fig. 3 collects the relaxed multilayer structures obtained stacking SiGe and the amorphous oxides with (SiGe/a-SiO_2, SiGe/a-SiO_2/a-SiON, and SiGe/a-SiO_2/a-SiON/a-HfO_2) and without (SiGe/a-HfO_2) the oxide interlayers. The direct contact between SiGe and a-HfO_2 (panel b) favors the formation of under-coordinated GeO_x and SiO_x pairs due to the presence of oxygen atoms at the interface. HfO_2 does not block the Ge diffusion of Ge across the surface favoring the formation of $HfGeO_x$ composites that are known to degrade the electrical quality of the interface by increasing the leakage current [45,93]. The comparison between the DOS spectra of SiGe surface and SiGe/a-HfO_2 interface (Fig 4a) confirms the experimental expectation [45]. The DOS plot shows the appearance of $HfGeO_x$-derived states that completely fill the pristine SiGe band gap and impart a conducting-like character to the interface. The presence of these states at the Fermi level (vertical dashed line in Fig 4) is responsible for the increase of the leakage current observed in the experiments.

Covering SiGe with the a-SiO_2 layer (panel c) allows for a better saturation of the surface Si atoms of SiGe and the reduction of the Si-O dangling bonds, as reported in Fig. S3. Although the amorphous oxide was generated by a melt-quench procedure rather than by explicitly modeling O_2 incorporation as in real devices [94], including the a-SiO_2 layer partially mimics the effect of the oxidation process by providing a stoichiometric SiO_2 environment that passivates Si bonds and reproduces the structural role of an interfacial oxide in real devices. Yet, a-SiO_2 is permeable to Ge that easily penetrates into the oxide layer forming undercoordinated $SiGeO_x$ mixed oxides. Structural analysis shows that Ge atoms migrate through the amorphous SiO_2 via interstitial-like hopping between transient free-volume pockets. These hops are enabled by bond-switching events in the Si–O network, in which Ge coordinates to non-bridging oxygens or replaces Si in a local Si–O unit, forming Ge–O bonds before moving onward. This is facilitated by the intrinsic disorder and variable ring sizes in amorphous silica, which provide low-coordination sites and diffusion channels absent in crystalline silica. Moreover, the analysis of Ge displacement along the Z-direction reported in Fig. 2 shows two main features: 1) the SiGe-SiO_2 interface modifies the vertical Ge distribution, with the formation of a Ge-rich region followed by a Ge-poor layer; 2) the formation of a Ge-rich region at the top of SiO2 IL, given by the Ge diffused atoms across the oxide. The Ge condensation at interface, that we observed through a total-energy-and-force structure relaxation, well agrees with the results of previous MD simulations [95], which show how Ge atoms aggregate at the oxide interface during the oxidation process characteristic of the SiGe fabrication.

To confirm the diffusion process and the stability of the obtained structure SiGe-SiO_2 interface, we performed two sets of Car-Parrinello ab initio dynamics (AIMD) at T = 300 K and T = 500 K for 10 ps each, to mimic working conditions and to accelerate dynamics. At both temperatures, the system remains stable (small values of Root Mean Square Fluctuations, RMSF, in Fig. 5a) with the same interatomic connectivity. The minor structural changes are only due to thermal fluctuations of atoms up to 0.5 Å, especially in the oxide region, having restrained the H-atoms at the bottom layer, as reported in Fig. 3a. In a similar way, also the small differences in the peak height of partial g(r) plots (Fig. 5b) from the relaxed (i.e. static) and AIMD simulations, are directly ascribable to the thermal fluctuations of atoms at finite temperatures.

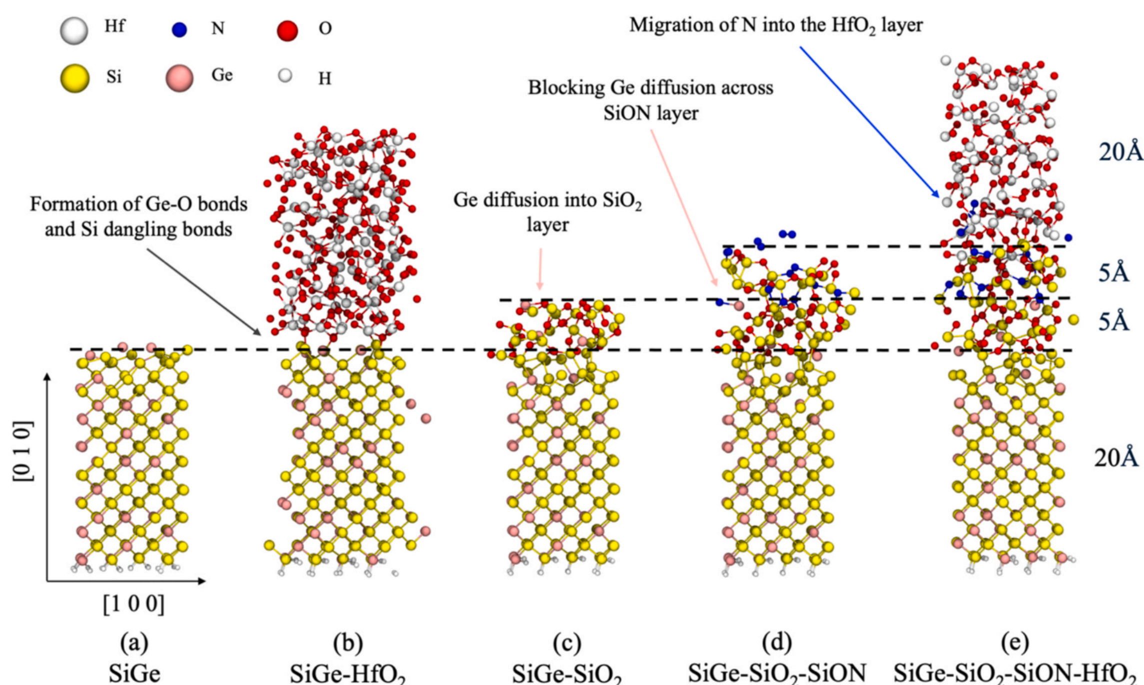

Fig. 3. Optimized atomic structure of SiGe surface and multiple SiGe/amorphous-oxide stacks.

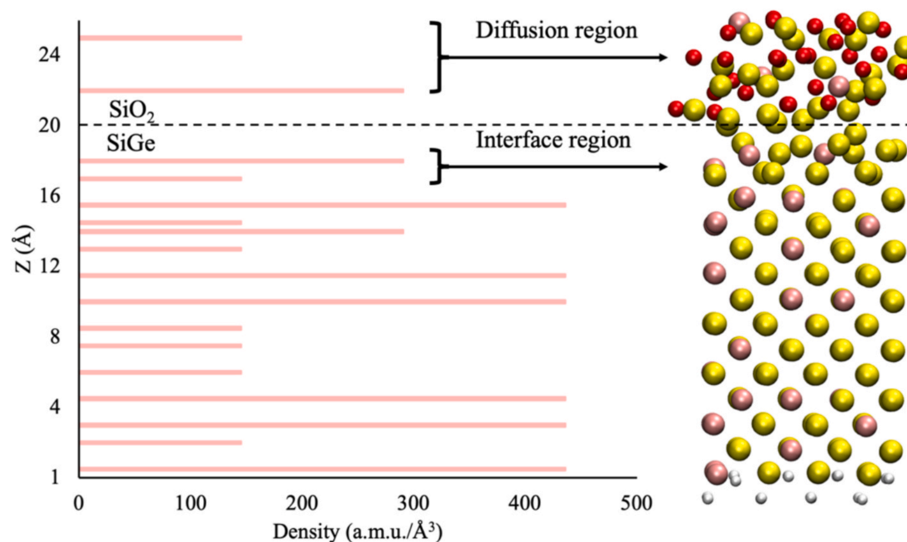

Fig. 4. Density of Ge atoms along the Z-direction where there are highlighted the Ge condensation at the interface region and the Ge atoms that diffuse into SiO_2 IL.

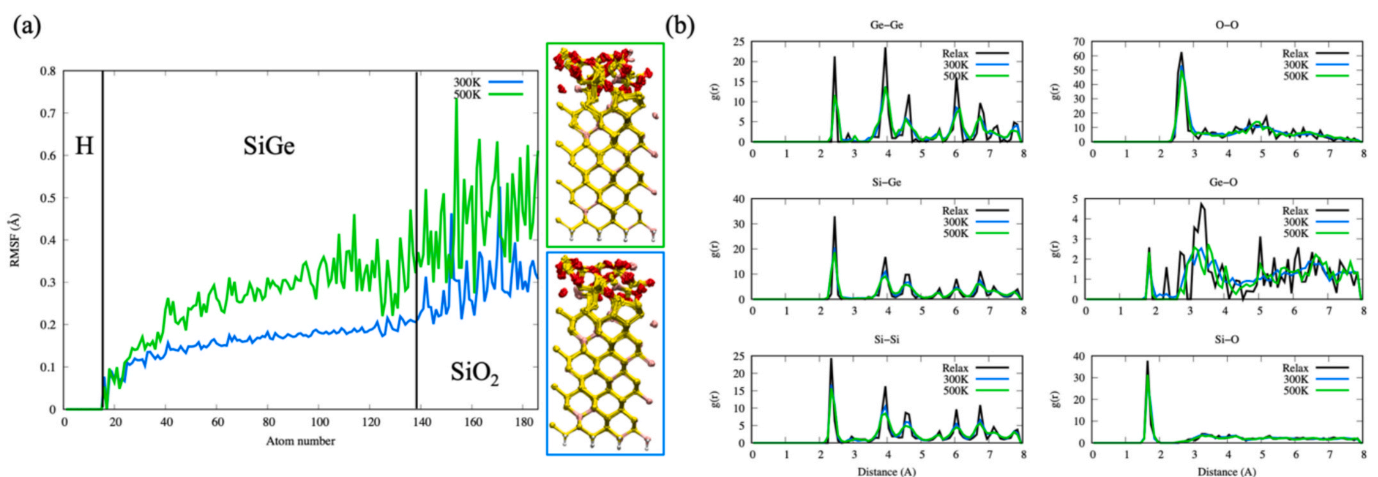

Fig. 5. (a) The RMSF and the superimposition of atomic structures at 300 K and 500 K AIMD. (b) The comparison of the partial g(r) at both temperatures and for the relaxed structure.

The mixture of GeO_x (parasitically unstable) and residual SiO_x could create interface-trapped charge density defects [37]. However, the electronic structure results (Fig. 6) indicate: **i.** the formation of a type-I band-alignment with the SiGe bandgap completely included in the a-SiO_2 one, **ii.** the absence of both Si- and Ge-derived defect states in the bandgap of the SiGe/a-SiO_2 interface, which preserves the energy gap (0.36 eV) of pristine SiGe. The analysis of the optimized structure indicates also the spontaneous diffusion of Ge atoms (pink balls) across the a-SiO_2 layer, with the Ge atoms that reach the upper surface of the oxide layer (Fig. 3c). This implies that – without further spacers – Ge could again be in touch with the a-HfO_2 surface, as in the binary interface. Thus, inclusion of a-SiO_2 is an efficient strategy to optimize the SiGe surface, but not to curate the Ge mobility. We obtained the spontaneous diffusion of Ge atoms with DFT relaxations without temperature effects, suggesting that our simulations take into account the kinetic effects.

The incorporation of a nitridation interfacial layer has been experimentally proved to prevent Ge diffusion into a-HfO_2 [45] and further improve the interface quality. Therefore, we added an amorphous oxynitride (a-SiON) interlayer on the top of SiGe/a-SiO_2 stack. The relaxed atomic configuration of the ternary multilayer is shown in Fig. 3(d). Upon structural relaxation, the a-SiON layer effectively inhibits the diffusion of Ge atoms across the interface due to its denser atomic structure, strong Si-N (1.71 Å) and Si-O (1.65 Å) bonding and low oxygen diffusivity [96]. Additionally, nitrogen partially diffuses into the lower SiO_2 layer as well as it segregates on the outermost layer, by forming N-N dimers weakly bonded to the top surface of the stack. The suppression of Ge diffusion by the oxynitride layer eventually prevents the undesirable formation of $HfGeO_x$ phases during subsequent stacking a-HfO_2, while the generation of N-N bonds may cause the establishment of further localized gap states near the Fermi level, which may impact the electronic properties of the interface. In fact, the DOS of the SiGe/a-SiO_2/a-SiON stack (Fig. 6c) displays a non insulating features, with a N-derived sharp peak laying at the Fermi level.

We finally re-introduced the a-HfO_2 on top of the previous stack to form SiGe/a-SiO_2/a- SiON/a-HfO_2 multilayer. The optimized structure is shown in Fig. 3(e). After relaxation, we observe significant intermixing between a-SiON and a-HfO_2, while Ge atoms remain segregated within the a-SiO_2 slab, as discussed above, obtaining an oxide layer (SiO_2-SiON) with thickness between 10Å and 11Å due to diffusivity phenomena. This minimizes the possibility to form the detrimental $HfGeO_x$ composites at the interface. Furthermore, the previous N-N dimers moved inside a-HfO_2 and formed 3-fold coordination with Hf atom. The N-N-Si-O bridge formed in lower SiGe/a-SiO_2/a-SiON interface migrated upwards, towards the a-HfO_2 layer, which gives rise to the

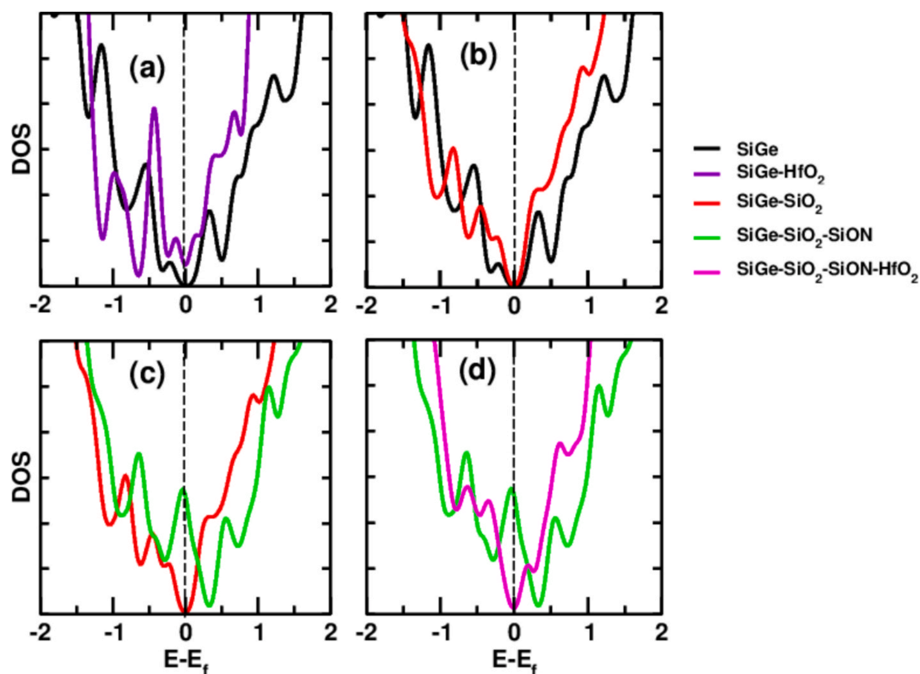

Fig. 6. Density of states for (a) $SiGe/HfO_2$ (b) $SiGe/a\text{-}SiO_2$ (c) $SiGe/a\text{-}SiO_2/a\text{-}SiON$, and (d) $SiGe/a\text{-}SiO_2/a\text{-}SiON/a\text{-}HfO_2$ multiple interfaces. Vertical dashed lines mark the Fermi energy (E_F) of each interface.

formation of two octahedral coordinated Hf atoms.

In order to gain further insights into the structural effects of the IL inclusion, we compared the $SiGe/HfO_2$ and the $SiGe/a\text{-}SiO_2/a\text{-}SiON/a\text{-}HfO_2$ interfaces. We computed the atomic density of each chemical along the *z*-axis (i.e. perpendicular to the multilayer), as reported in Fig. 7. In $SiGe/HfO_2$, the different chemical composition prevents any bond continuity across the interface and the formation of under-coordinated sub-composites. In the complete system, we observe a smoother interface region that maximizes the suppression of under- coordinated sites and dangling bonds. In particular, the first SiO_2 maintains the continuity of Si-bonds and introduces oxygen that is the common element also of the remaining layers. Ge partially diffuses in the SiO_2 layer, remaining

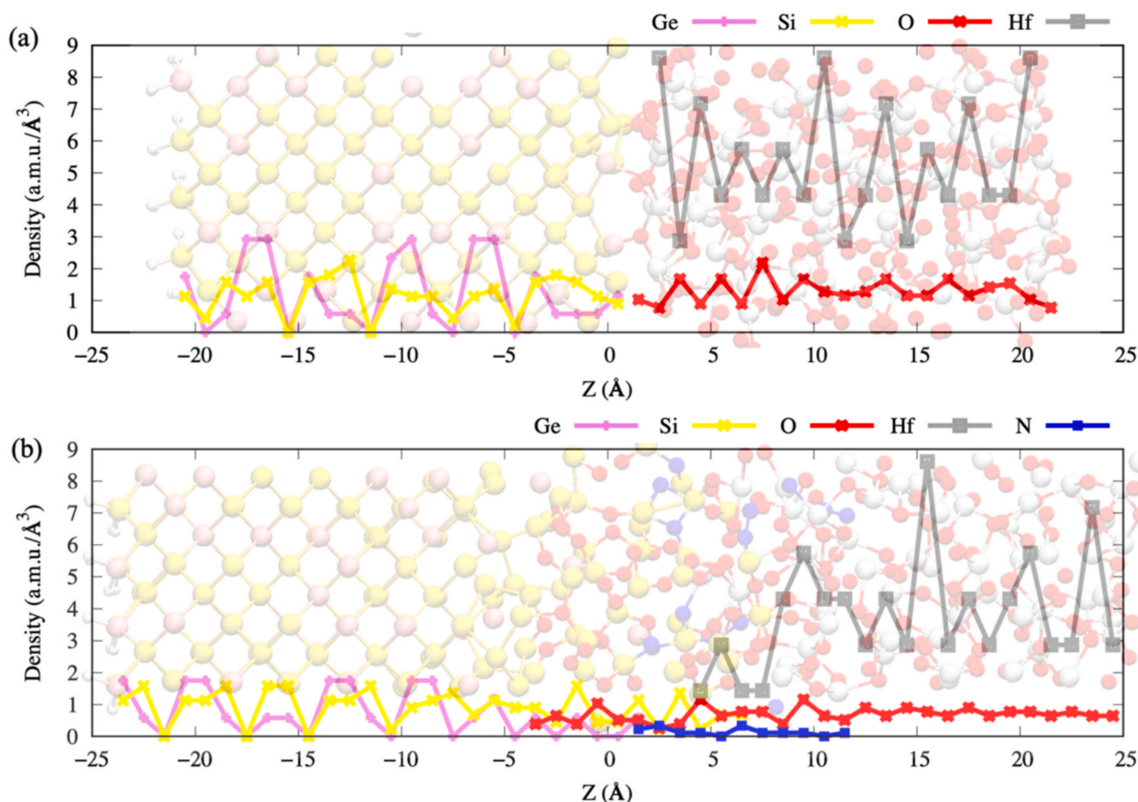

Fig. 7. Atomic density distribution of each chemical species along the *z*-direction for (a) $SiGe/HfO_2$ and (b) the $SiGe/SiO_2/SiON/HfO_2$ interfaces.

blocked within a-SiON. Hf slightly diffuses into the a-SiON layer, but without reaching the Ge-diffusion region, while N spatially spreads over 10 Å between SiO_2 and HfO_2, i.e. doubling the 5 Å thickness of the initial structure.

The different bonding path and the local order redistribution can be quantified by computing the q-value parameter, which is a measure of the local disorder around each atom based on the first shell of neighbors, by using the BELLO code [97,98]. The q-value is defined as:

$$q = 1 - \frac{3}{8}\sum_{k>i}\left(\frac{1}{3} + coscos\theta_{ijk}\right)^2 \tag{1}$$

where θ_{ijk} is the angle formed by atoms i and k with the central atom j. The local order parameter can assume values from 1, (perfect tetrahedral network) to 0 (six-fold octahedral network) and to -2 (six-fold non-octahedral network). The q-value for the $SiGe/HfO_2$ systems has a large jump from 1 in the crystalline SiGe to the disordered HfO_2, where the q-values have a large distribution, see Fig. 8. In the case of $SiGe/SiO_2/SiON/HfO_2$, the q-value is 1 in the SiGe region and decreases much more smoothly in the SiO_2 layer.

This multiple atom rearrangement has a positive effect on the electronic properties of the overall multilayer, as indicated by the DOS spectra in Fig. 6(d). The complete stack recovers the expected insulating character, with an energy gap of 0.31 eV associated to the SiGe channel. Neither SiO_x nor $HfGeO_x$ derived states appear in the SiGe bandgap: the inclusion of the a-HfO_2 saturates the N-N dangling bonds emptying the bandgap. O-derived localized states, associated to outermost a-HfO_2 are detected far from the Fermi energy, well inside the valence band.

Fig. 9(a) shows the charge density difference $\Delta\rho(z)$ along the z-direction, defined as the difference between the charge density of the complete stack and of those of the single layers:

$$\Delta\rho = \rho(SiGe/SiO_2/SiON/HfO_2) - \rho(SiGe) - \rho(SiO_2) - \rho(SiON) - \rho(HfO_2) \tag{2}$$

At the SiGe/a-SiO_2 interface $\Delta\rho(z)$ has a large negative value, which indicates a net charge transfer from SiGe to a-SiO_2 and the formation of an interfacial dipole. The remaining part of the multistack exhibits a charge accumulation at the single oxide/oxide interfaces. The PDOS of Fig. 9(b) shows that the SiGe band gap (in green) is fully enclosed within the HfO2 band gap, evidencing a type-I band alignment and no interface-induced mid-gap states are observed within the SiGe band gap.

4. Conclusion

We have examined the effects of multiple interlayers insertion between $Si_{0.75}Ge_{0.25}$ and a-HfO_2 oxide with the aim of reducing the formation of GeO_x and $HfGeO_x$ composites, eliminating Ge out-diffusion, and subsequently creating a defect-free interface. Our results revealed that combining SiGe and a-SiO_2 oxide as the first interlayer, Ge atoms are able to migrate into the $aSiO_2$ which resulted into the formation of $SiGeO_x$ mixed oxides. The introduction of a second interlayer (a-SiON oxide) is able to block the Ge diffusion but it caused the appearance of defect trap states that could negatively increase the leakage current. The complete stacking arrangement SiGe/a-SiO_2/a-SiON/a-HfO_2 shows a type-I band alignment, restores the necessary semiconducting character of the interface whilst protecting the HfO2 layer from Ge and the generation of $HfGeO_x$ micro-composites. We can thus conclude that, despite a greater structural complexity, the insertion of multiple interlayers between SiGe and a-HfO_2 oxide is an efficient solution to obtain high quality high-κ oxide gate stacks for p-MOSFET applications. Our results allow to optimize strategies to reduce leakage currents and device instabilities induced by Ge migration at the high-k oxide in p-MOSFETs, without altering much the device engineering cost due to the increased structural complexity. This is a necessary step towards the realization of efficient p-MOSFET hole qubits.

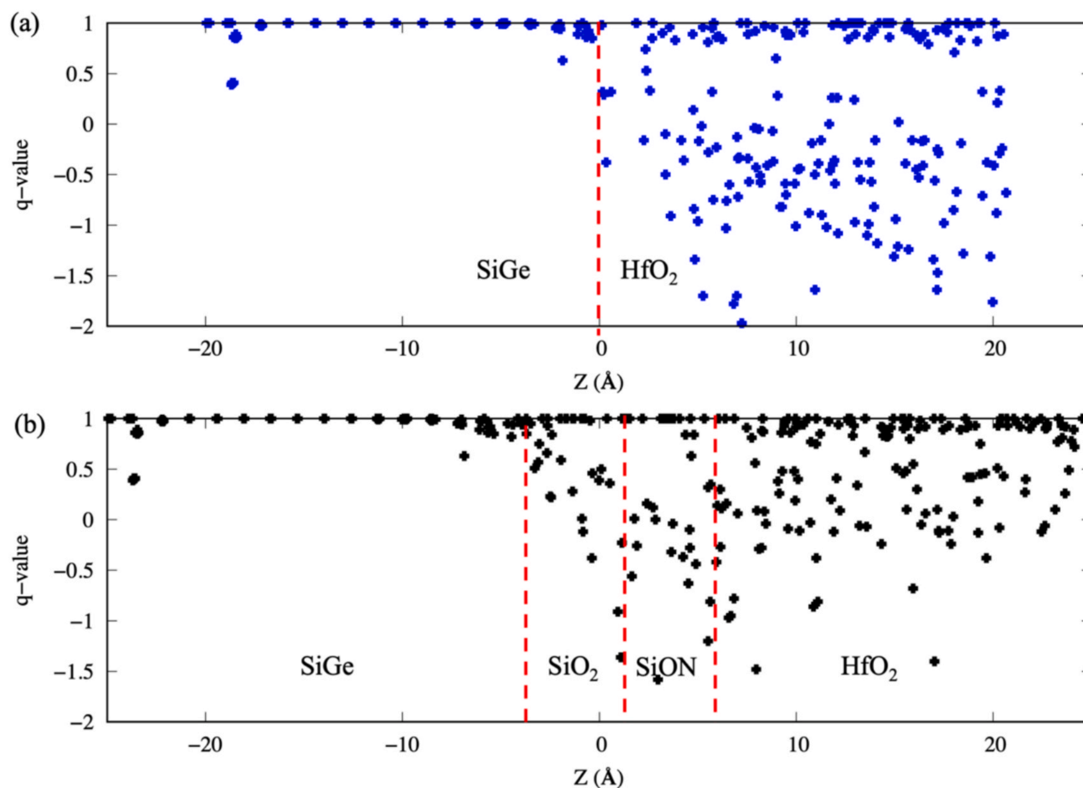

Fig. 8. The q-value distribution along the z-direction for (a) $SiGe/HfO_2$ and (b) the $SiGe/SiO_2/SiON/HfO_2$ interfaces. Red vertical lines identify the spatial position of the interfaces along the z-axis.

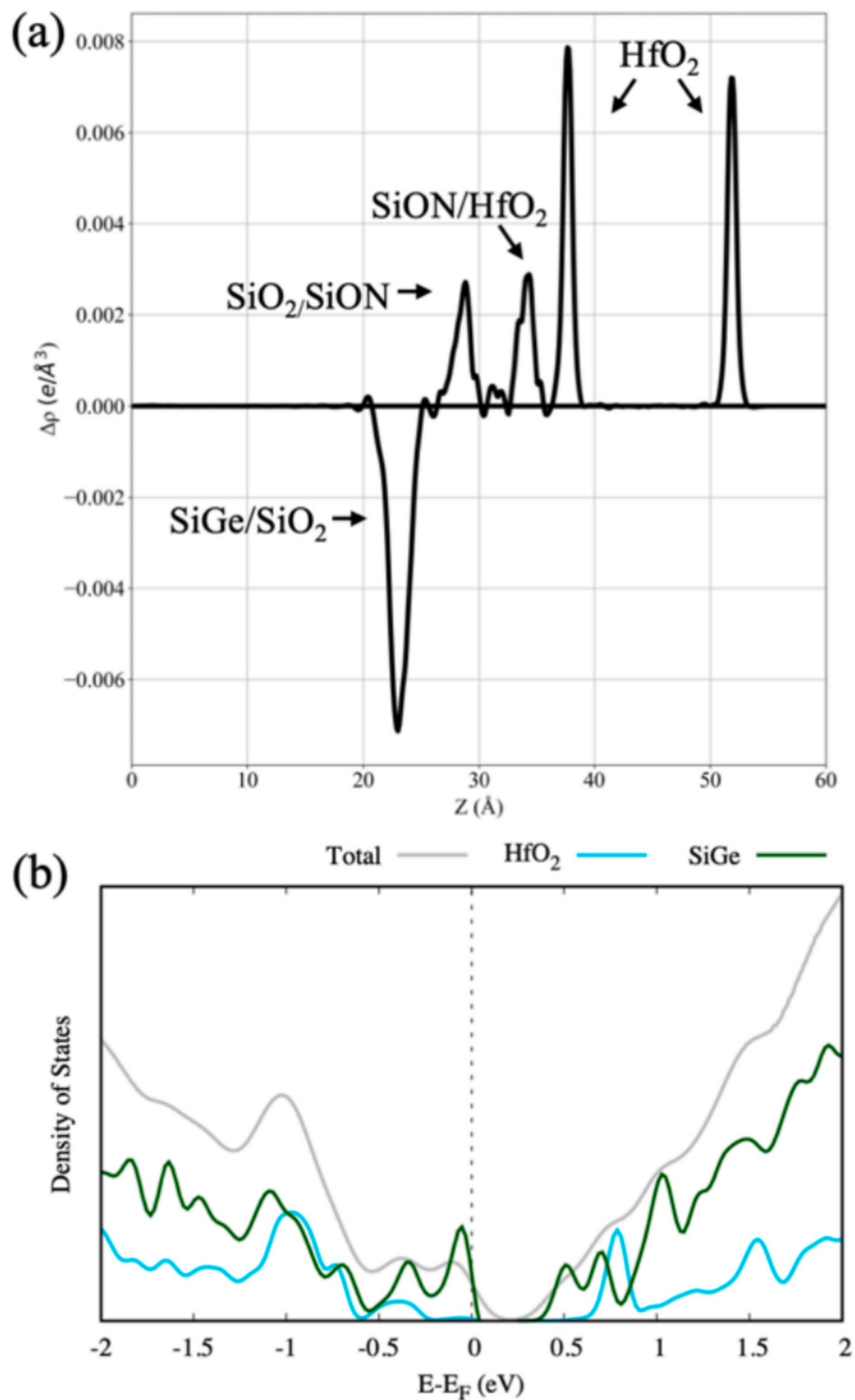

Fig. 9. (a) Charge density difference profile along the *z*-direction, across the SiGe/a-SiO_2/a-SiON/a-HfO_2 interface. (b) Local PDOS of SiGe and HfO_2 in the interface system showing that SiGe lies in the band gap of HfO_2.

CRediT authorship contribution statement

Ibrahim B. Adetunji: Writing – original draft, Investigation, Formal analysis, Data curation. **Francesco Tavanti:** Writing – review & editing, Investigation. **Alessandra Catellani:** Writing – review & editing, Supervision. **Arrigo Calzolari:** Writing – review & editing, Supervision, Conceptualization.

Declaration of competing interest

The authors declare that they have no known competing financial interests or personal relationships that could have appeared to influence the work reported in this paper.

Acknowledgements

This work was supported by the iQubits project (EU Project H2020-FETOpen-829005). BIA acknowledges Dr. Winnie Mulwa of Department of Physics, Egerton University, Kenya, and the Centre for High Performance Computing (CHPC) South Africa for part of the computational resources (MATS1181). The authors also acknowledge the support of the CINECA HPC center (ITA) through project Iscra-B IsC80_i-Qubits.

Appendix A. Supplementary data

Supplementary data to this article can be found online at https://doi.org/10.1016/j.apsusc.2025.165552.

Data availability

Data will be made available on request.

References

[1] M.A. Eriksson, SiGe: materials and devices for quantum computing?, in: 2006 Int. SiGe Technol. Device Meet., 2006, p. 1, https://doi.org/10.1109/ISTDM.2006.246528.

[2] M. Xiao, M.G. House, H.W. Jiang, Measurement of the spin relaxation time of single electrons in a silicon metal-oxide-semiconductor-based quantum dot, Phys. Rev. Lett. 104 (2010) 096801, https://doi.org/10.1103/PhysRevLett.104.096801.

[3] B.M. Maune, M.G. Borselli, B. Huang, T.D. Ladd, P.W. Deelman, K.S. Holabird, A. A. Kiselev, I. Alvarado-Rodriguez, R.S. Ross, A.E. Schmitz, M. Sokolich, C. A. Watson, M.F. Gyure, A.T. Hunter, Coherent singlet-triplet oscillations in a silicon-based double quantum dot, Nature 481 (2012) 344–347, https://doi.org/10.1038/nature10707.

[4] E. Kawakami, T. Jullien, P. Scarlino, D.R. Ward, D.E. Savage, M.G. Lagally, V. V. Dobrovitski, M. Friesen, S.N. Coppersmith, M.A. Eriksson, L.M.K. Vandersypen, Gate fidelity and coherence of an electron spin in an Si/SiGe quantum dot with micromagnet, Proc. Natl. Acad. Sci. 113 (2016) 11738–11743, https://doi.org/10.1073/pnas.1603251113.

[5] M.H. Devoret, A. Wallraff, J.M. Martinis, Superconducting qubits: a short review, (2004). https://doi.org/10.48550/arXiv.cond-mat/0411174.

[6] L.M.K. Vandersypen, H. Bluhm, J.S. Clarke, A.S. Dzurak, R. Ishihara, A. Morello, D. J. Reilly, L.R. Schreiber, M. Veldhorst, Interfacing spin qubits in quantum dots and donors—hot, dense, and coherent, npj Quantum Inf. 3 (2017) 34, https://doi.org/10.1038/s41534-017-0038-y.

[7] E.E. McCluskey Matthew, D. Haller. Dopants and Defects in Semiconductors, CRC Press, 2012, ISBN 978-1439831533.

[8] J. Golio Mike, R.F. Golio. Microwave Passive and Active Technologies, CRC Press, 2018.

[9] J. Franco, B. Kaczer, G. Groeseneken. Reliability of High Mobility SiGe Channel MOSFETs for Future CMOS Applications, Springer Netherlands, Dordrecht, 2014, https://doi.org/10.1007/978-94-007-7663-0.

[10] S. Bonen, U. Alakusu, Y. Duan, M.J. Gong, M.S. Dadash, L. Lucci, D.R. Daughton, G. C. Adam, S. Iordănescu, M. Păşteanu, I. Giangu, H. Jia, L.E. Gutierrez, W.T. Chen, N. Messaoudi, D. Harame, A. Müller, R.R. Mansour, P. Asbeck, S.P. Voinigescu, Cryogenic characterization of 22-nm FDSOI CMOS technology for quantum computing ICs, IEEE Electron Device Lett. 40 (2019) 127–130, https://doi.org/10.1109/LED.2018.2880303.

[11] V. Sridharan, K. Pudi. Design of Arithmetic Circuits in Quantum Dot Cellular Automata Nanotechnology, Springer, 2015, ISBN 978-3319166889.

[12] M. Ieong, B. Doris, J. Kedzierski, K. Rim, M. Yang, Silicon device scaling to the sub-10-nm regime, Science 306 (2004) 2057–2060.

[13] K. Lee, I. Nam, I. Kwon, J. Gil, K. Han, S. Park, B.-I. Seo, The impact of semiconductor technology scaling on CMOS RF and digital circuits for wireless application, IEEE Trans. Electron Devices 52 (2005) 1415–1422, https://doi.org/10.1109/TED.2005.850632.

[14] A. Moshovos, G.S. Sohi, Microarchitectural innovations: Boosting microprocessor performance beyond semiconductor technology scaling, Proc. IEEE 89 (2001) 1560–1575.

[15] G.D. Wilk, R.M. Wallace, J.M. Anthony, High-κ gate dielectrics: current status and materials properties considerations, J. Appl. Phys. 89 (2001) 5243–5275, https://doi.org/10.1063/1.1361065.

[16] E.P. Gusev, V. Narayanan, M.M. Frank, Advanced high-κ dielectric stacks with polySi and metal gates: recent progress and current challenges, IBM J. Res. Dev. 50 (2006) 387–410, https://doi.org/10.1147/rd.504.0387.

[17] K.J. Kuhn, Considerations for ultimate CMOS scaling, IEEE Trans. Electron Devices 59 (2012) 1813–1828, https://doi.org/10.1109/TED.2012.2193129.

[18] K.A.R. Dennis, W. Hess. Handbook of Silicon Wafer Cleaning Technology, William Andrew Inc., 2008, ISBN 978-0-8155-1554-8.

[19] S.E. Thompson, M. Armstrong, C. Auth, S. Cea, R. Chau, G. Glass, T. Hoffman, J. Klaus, Z. Ma, B. Mcintyre, et al., A logic nanotechnology featuring strained-silicon, IEEE Electron Device Lett. 25 (2004) 191–193.

[20] B. Cheng, C. Li, Z. Liu, C. Xue, Research progress of Si-based germanium materials and devices, J. Semicond. 37 (2016) 081001, https://doi.org/10.1088/1674-4926/37/8/081001.

[21] H.-Y. Yu, M. Ishibashi, J.-H. Park, M. Kobayashi, K.C. Saraswat, p-Channel Ge MOSFET by selectively heteroepitaxially grown Ge on Si, IEEE Electron Device Lett. 30 (2009) 675–677, https://doi.org/10.1109/LED.2009.2019847.

[22] K. Yu, F. Yang, H. Cong, L. Zhou, Q. Liu, L. Zhang, B. Cheng, C. Xue, Y. Zuo, C. Li, Fabrication of high-hole-mobility germanium-on-insulator wafers through an easy method, J. Alloys Compd. 750 (2018) 182–188.

[23] J.L. Hoyt, H.M. Nayfeh, S. Eguchi, I. Aberg, G. Xia, T. Drake, E.A. Fitzgerald, D. A. Antoniadis, Strained silicon MOSFET technology, in: Dig. Int. Electron Devices Meet., 2002, pp. 23–26, https://doi.org/10.1109/IEDM.2002.1175770.

[24] O. Weber, J.-F. Damlencourt, F. Andrieu, F. Ducroquet, T. Ernst, J.-M. Hartmann, A.-M. Papon, O. Renault, B. Guillaumot, S. Deleonibus, Fabrication and mobility characteristics of SiGe surface channel pMOSFETs with a HfO/sub 2//TiN gate stack, IEEE Trans. Electron Devices 53 (2006) 449–456, https://doi.org/10.1109/TED.2005.863536.

[25] W. Yu, B. Zhang, C. Liu, Y. Zhao, W.R. Wu, Z.Y. Xue, M. Chen, D. Buca, J.-M. Hartmann, X. Wang, Q.T. Zhao, S. Mantl, Impact of Si cap, strain and temperature on the hole mobility of (s)Si/sSiGe/(s)SOI quantum-well p-MOSFETs, Microelectron. Eng. 113 (2014) 5–9, https://doi.org/10.1016/j.mee.2013.06.015.

[26] D. Lu, P. Morin, B. Sahu, T.B. Hook, P. Hashemi, A. Scholze, B. Kim, P. Kerber, A. Khakifirooz, P. Oldiges, et al., Silicon germanium FinFET device physics, process integration and modeling considerations, ECS Trans. 64 (2014) 337.

[27] P. Hashemi, K. Balakrishnan, S.U. Engelmann, J.A. Ott, A. Khakifirooz, A. Baraskar, M. Hopstaken, J.S. Newbury, K.K. Chan, E. Leobandung, et al., First demonstration of high-Ge-content strained-Si 1- x Ge x (x= 0.5) on insulator PMOS FinFETs with high hole mobility and aggressively scaled fin dimensions and gate lengths for high-performance applications, in: 2014 IEEE Int. Electron Devices Meet., IEEE, 2014, p. 16.

[28] D. Fischer, A. Kersch, The effect of dopants on the dielectric constant of HfO2 and ZrO2 from first principles, Appl. Phys. Lett. 92 (2008) 012908.

[29] T. Ando, P. Hashemi, J. Bruley, J. Rozen, Y. Ogawa, S. Koswatta, K.K. Chan, E. A. Cartier, R. Mo, V. Narayanan, High mobility high-Ge-content SiGe PMOSFETs using Al2O3/HfO2 stacks with In-Situ O3 treatment, IEEE Electron Device Lett. 38 (2017) 303–305.

[30] Z.-Z. Hou, G.-L. Wang, J.-J. Xiang, J.-X. Yao, Z.-H. Wu, Q.-Z. Zhang, H.-X. Yin, Improved operation characteristics for nonvolatile charge-trapping memory capacitors with high-κ dielectrics and SiGe epitaxial substrates, Chin. Phys. Lett. 34 (2017) 097304.

[31] L. Kornblum, Conductive oxide interfaces for field effect devices, Adv. Mater. Interfaces 6 (2019) 1900480.

[32] Y.-L. Li, K.-S. Chang-Liao, C.-C. Li, H.-T. Feng, C.-H. Kao, C.-Y. Chen, D.-B. Ruan, Y.-J. Chen, K.-S. Li, G.-L. Luo, Improved electrical characteristics of bulk FinFETs with SiGe super-lattice-like buried channel, IEEE Electron Device Lett. 40 (2019) 181–184.

[33] J. Robertson, R.M. Wallace, High-K materials and metal gates for CMOS applications, Mater. Sci. Eng. R. Rep. 88 (2015) 1–41.

[34] X. Ma, J. Xiang, L. Zhou, X. Wang, Y. Li, H. Yang, J. Zhang, C. Zhao, H. Yin, W. Wang, et al., Comprehensive study and design of high-k/SiGe gate stacks with interface-engineering by ozone oxidation, ECS J. Solid State Sci. Technol. 8 (2019) N100.

[35] S. Kol, A. Oral, Hf-based high-κ dielectrics: a review, Acta Phys. Pol. A (2019) 136.

[36] M.C. Cheynet, S. Pokrant, F.D. Tichelaar, J.-L. Rouvière, Crystal structure and band gap determination of HfO2 thin films, J. Appl. Phys. 101 (2007) 054101.

[37] E.A. Chagarov, M.S. Kavrik, Z. Fang, W. Tsai, A.C. Kummel, Density-functional theory molecular dynamics simulations of a-HfO2/a-SiO2/SiGe and a-HfO2/a-SiO2/Ge with a-SiO2 and a-SiO suboxide interfacial layers, Appl. Surf. Sci. 443 (2018) 644–654, https://doi.org/10.1016/j.apsusc.2018.02.041.

[38] M.-H. Cho, H. Chang, D. Moon, S. Kang, B. Min, D.-H. Ko, H. Kim, P.C. McIntyre, J. H. Lee, J. Ku, et al., Interfacial characteristics of HfO 2 films grown on strained Si 0.7 Ge 0.3 by atomic-layer deposition, Appl. Phys. Lett. 84 (2004) 1171–1173.

[39] K. Prabhakaran, F. Maeda, Y. Watanabe, T. Ogino, Thermal decomposition pathway of Ge and Si oxides: observation of a distinct difference, Thin Solid Films 369 (2000) 289–292.

[40] L. Zhang, Y. Guo, V.V. Hassan, K. Tang, M.A. Foad, J.C. Woicik, P. Pianetta, J. Robertson, P.C. McIntyre, Interface engineering for atomic layer deposited alumina gate dielectric on SiGe substrates, ACS Appl. Mater. Interfaces 8 (2016) 19110–19118.

[41] P. Hashemi, T. Ando, K. Balakrishnan, E. Cartier, M. Lofaro, J. Ott, J. Bruley, K.-L. Lee, S. Koswatta, S. Dawes, et al., Replacement high-K/metal-gate High-Ge-content strained SiGe FinFETs with high hole mobility and excellent SS and reliability at aggressive EOT 7Å and scaled dimensions down to sub-4nm fin widths, in: 2016 IEEE Symp. VLSI Technol., IEEE, 2016, pp. 1–2.

[42] M.S. Kavrik, A. Bostwick, E. Rotenberg, K. Tang, E. Thomson, T. Aoki, B. Fruhberger, Y. Taur, P.C. McIntyre, A.C. Kummel, Understanding the mechanism of electronic defect suppression enabled by nonidealities in atomic layer deposition, J. Am. Chem. Soc. 142 (2019) 134–145.

[43] C. Lee, H. Kim, P. Jamison, R. Southwick, S. Mochizuki, K. Watanabe, R. Bao, R. Galatage, S. Guillaumet, T. Ando, et al., Selective GeO x-scavenging from interfacial layer on Si 1- x Ge x channel for high mobility Si/Si 1- x Ge x CMOS application, in: 2016 IEEE Symp. VLSI Technol., IEEE, 2016, pp. 1–2.

[44] W.-L. Lee, C.-Y. Yu, J.-L. Zhang, G.-L. Luo, C.-H. Chien, Improving interface state density and thermal stability of high-kappa gate stack through high-vacuum annealing on Si 0.5 Ge 0.5, IEEE Electron Device Lett. 40 (2019) 678–681.

[45] N. Lu, W. Bai, A. Ramirez, C. Mouli, A. Ritenour, M.L. Lee, D. Antoniadis, D. L. Kwong, Ge diffusion in Ge metal oxide semiconductor with chemical vapor deposition HfO2 dielectric, Appl. Phys. Lett. 87 (2005) 051922, https://doi.org/10.1063/1.2001757.

[46] Q. Zhang, N. Wu, D.M.Y. Lai, Y. Nikolai, L. Bera, C. Zhu, Germanium incorporation in HfO2 dielectric on germanium substrate, J. Electrochem. Soc. 153 (2006) G207.

[47] Q.-Q. Sun, Y. Shi, L. Dong, H. Liu, S.-J. Ding, D.W. Zhang, Impact of germanium related defects on electrical performance of hafnium oxide, Appl. Phys. Lett. 92 (2008) 102908.

[48] S. Da Silva, G.K. Rolim, G.V. Soares, I.J.R. Baumvol, C. Krug, L. Miotti, F. Freire Jr, M. Da Costa, C. Radtke, Oxygen transport and GeO2 stability during thermal oxidation of Ge, Appl. Phys. Lett. 100 (2012) 191907.

[49] S. Ogawa, R. Asahara, Y. Minoura, H. Sako, N. Kawasaki, I. Yamada, T. Miyamoto, T. Hosoi, T. Shimura, H. Watanabe, Insights into thermal diffusion of germanium and oxygen atoms in HfO2/GeO2/Ge gate stacks and their suppressed reaction with atomically thin AlOx interlayers, J. Appl. Phys. 118 (2015) 235704.

[50] X. Li, Y. Noma, W. Song, T. Nishimura, A. Toriumi, Interface reaction kinetics in SiGe oxidation, Appl. Phys. Lett. 115 (2019) 232901.

[51] M.S. Kavrik, P. Ercius, J. Cheung, K. Tang, Q. Wang, B. Fruhberger, M. Kim, Y. Taur, P.C. McIntyre, A.C. Kummel, Engineering High-k/SiGe interface with ALD oxide for selective GeO x reduction, ACS Appl. Mater. Interfaces 11 (2019) 15111–15121.

[52] M.S. Kavrik, E. Thomson, E. Chagarov, K. Tang, S.T. Ueda, V. Hou, T. Aoki, M. Kim, B. Fruhberger, Y. Taur, et al., Ultralow defect density at sub-0.5 nm HfO2/SiGe interfaces via selective oxygen scavenging, ACS Appl. Mater. Interfaces 10 (2018) 30794–30802.

[53] K. Sardashti, K.-T. Hu, K. Tang, S. Madisetti, P. McIntyre, S. Oktyabrsky, S. Siddiqui, B. Sahu, N. Yoshida, J. Kachian, others, Nitride passivation of the interface between high-k dielectrics and SiGe, Appl. Phys. Lett. 108 (2016) 011604.

[54] J.-H. Han, M. Takenaka, S. Takagi, Analysis of interface trap density of plasma post-nitrided Al2O3/SiGe MOS interface with high Ge content using high-temperature conductance method, J. Appl. Phys. 120 (2016) 125707.

[55] J. Huang, N. Wu, Q. Zhang, C. Zhu, M. Li, A.A. Tay, Z.-Y. Cheng, C.W. Leitz, A. Lochtefeld, Surface NH 3 anneal on strained Si 0.5 Ge 0.5 for metal-oxide-semiconductor applications with Hf O 2 as gate dielectric, Appl. Phys. Lett. 88 (2006) 143506.

[56] K. Sardashti, K.-T. Hu, K. Tang, S. Park, H. Kim, S. Madisetti, P. McIntyre, S. Oktyabrsky, S. Siddiqui, B. Sahu, et al., Sulfur passivation for the formation of Si-terminated Al2O3/SiGe (0 0 1) interfaces, Appl. Surf. Sci. 366 (2016) 455–463.

[57] Q. Yao, X. Ma, H. Wang, Y. Wang, G. Wang, J. Zhang, W. Liu, X. Wang, J. Yan, Y. Li, W. Wang, Investigate on the mechanism of HfO2/Si0.7Ge0.3 interface passivation based on low-temperature ozone oxidation and Si-Cap methods, Nanomaterials 11 (2021).

[58] Z. Chen, Z. Lan, Y. Lin, T. Nishimura, C. Lee, Y. Zhao, Optimizing interface properties of HfO2/Si0.73Ge0.27 gate stacks through sulfur passivation and post-deposition annealing, J. Appl. Phys. 135 (2024) 125704.

[59] S. Krishnan, U. Kwon, N. Moumen, M.W. Stoker, E.C.T. Harley, S. Bedell, D. Nair, B. Greene, W. Henson, M. Chowdhury, D.P. Prakash, E. Wu, D. Ioannou, E. Cartier, M.H. Na, S. Inumiya, K. Mcstay, L. Edge, R. Iijima, J. Cai, M. Frank, M. Hargrove, D. Guo, A. Kerber, H. Jagannathan, T. Ando, J. Shepard, S. Siddiqui, M. Dai, H. Bu, J. Schaeffer, D. Jaeger, K. Barla, T. Wallner, S. Uchimura, Y. Lee, G. Karve, S. Zafar, D. Schepis, Y. Wang, R. Donaton, S. Saroop, P. Montanini, Y. Liang, J. Stathis, R. Carter, R. Pal, V. Paruchuri, H. Yamasaki, J.-H. Lee, M. Ostermayr, J.-P. Han, Y. Hu, M. Gribelyuk, D.G. Park, X. Chen, S. Samavedam, S. Narasimha, P. Agnello, M. Khare, R. Divakaruni, V. Narayanan, M. Chudzik, A manufacturable dual channel (Si and SiGe) high-k metal gate CMOS technology with multiple oxides for high performance and low power applications, in: 2011 IEEE Int. Electron Devices Meet. IEDM, IEEE, 2011, pp. 28.1.1–28.1.4.

[60] B.P. Linder, E.A. Cartier, S. Krishnan, (Invited) metal gate/high- dielectric gate stack reliability; or How I learned to live with trappy oxides, ECS Trans. 53 (2013) 187–192.

[61] P. Giannozzi, S. Baroni, N. Bonini, M. Calandra, R. Car, C. Cavazzoni, D. Ceresoli, G.L. Chiarotti, M. Cococcioni, I. Dabo, others, QUANTUM ESPRESSO: a modular and open-source software project for quantum simulations of materials, J. Phys. Condens. Matter 21 (2009) 395502.

[62] P. Giannozzi, O. Andreussi, T. Brumme, O. Bunau, M. Buongiorno Nardelli, M. Calandra, R. Car, C. Cavazzoni, D. Ceresoli, M. Cococcioni, N. Colonna, I. Carnimeo, A. Dal Corso, S. de Gironcoli, P. Delugas, R.A. DiStasio, A. Ferretti, A. Floris, G. Fratesi, G. Fugallo, R. Gebauer, U. Gerstmann, F. Giustino, T. Gorni, J. Jia, M. Kawamura, H.-Y. Ko, A. Kokalj, E. Küçükbenli, M. Lazzeri, M. Marsili, N. Marzari, F. Mauri, N.L. Nguyen, H.-V. Nguyen, A. Otero-de-la-Roza, L. Paulatto, S. Poncé, D. Rocca, R. Sabatini, B. Santra, M. Schlipf, A.P. Seitsonen, A. Smogunov, I. Timrov, T. Thonhauser, P. Umari, N. Vast, X. Wu, S. Baroni, Advanced capabilities for materials modelling with quantum ESPRESSO, J. Phys. Condens. Matter 29 (2017) 465901, https://doi.org/10.1088/1361-648X/aa8f79.

[63] P. Giannozzi, O. Baseggio, P. Bonfà, D. Brunato, R. Car, I. Carnimeo, C. Cavazzoni, S. de Gironcoli, P. Delugas, F. Ferrari Ruffino, A. Ferretti, N. Marzari, I. Timrov, A. Urru, S. Baroni, Quantum ESPRESSO toward the exascale, J. Chem. Phys. 152 (2020) 154105, https://doi.org/10.1063/5.0005082.

[64] J.P. Perdew, K. Burke, M. Ernzerhof, Generalized gradient approximation made simple, Phys. Rev. Lett. 77 (1996) 3865–3868, https://doi.org/10.1103/PhysRevLett.77.3865.

[65] D. Vanderbilt, Soft self-consistent pseudopotentials in a generalized eigenvalue formalism, Phys. Rev. B 41 (1990) 7892–7895, https://doi.org/10.1103/PhysRevB.41.7892.

[66] M. Cococcioni, S. de Gironcoli, Linear response approach to the calculation of the effective interaction parameters in the LDA + U method, Phys. Rev. B 71 (2005) 035105, https://doi.org/10.1103/PhysRevB.71.035105.

[67] L.A. Agapito, S. Curtarolo, M. Buongiorno Nardelli, Reformulation of DFT + U as a pseudohybrid hubbard density functional for accelerated materials discovery, Phys. Rev. X 5 (2015) 1–16.

[68] A.R. Supka, T.E. Lyons, L. Liyanage, P. D'Amico, R.A.R. Al Orabi, S. Mahatara, P. Gopal, C. Toher, D. Ceresoli, A. Calzolari, et al., AFLOWπ: a minimalist approach to high-throughput ab initio calculations including the generation of tight-binding hamiltonians, Comput. Mater. Sci 136 (2017) 76–84.

[69] A. Calzolari, M.B. Nardelli, Dielectric properties and Raman spectra of ZnO from a first principles finite-differences/finite-fields approach, Sci. Rep. 3 (2013) 2999.

[70] P. Gopal, M. Fornari, S. Curtarolo, L.A. Agapito, L.S.I. Liyanage, M. Buongiorno Nardelli, Improved predictions of the physical properties of Zn- and Cd-based wide band-gap semiconductors: a validation of the ACBN0 functional, Phys. Rev. B 91 (2015) 245202–245209.

[71] M. Breeden, S. Wolf, S. Ueda, Z. Fang, C.-Y. Chang, K. Tang, P. McIntyre, A. C. Kummel, Al2O3, Si0.7Ge0.3(001) & HfO2/Si0.7Ge0.3(001) interface trap state reduction via in-situ N2/H2 RF downstream plasma passivation, Appl. Surf. Sci. 478 (2019) 1065–1073, https://doi.org/10.1016/j.apsusc.2019.01.216.

[72] X. Li, W. Song, K. Yang, N.A. Krishnan, B. Wang, M.M. Smedskjaer, J.C. Mauro, G. Sant, M. Balonis, M. Bauchy, Cooling rate effects in sodium silicate glasses: Bridging the gap between molecular dynamics simulations and experiments, J. Chem. Phys. 147 (2017) 074501.

[73] J.D. Gale, GULP: a computer program for the symmetry-adapted simulation of solids, J. Chem. Soc. Faraday Trans. 93 (1997) 629–637, https://doi.org/10.1039/A606455H.

[74] A. Pedone, G. Malavasi, M.C. Menziani, A.N. Cormack, U. Segre, A new self-consistent empirical interatomic potential model for oxides, silicates, and silica-based glasses, J. Phys. Chem. B 110 (2006) 11780–11795, https://doi.org/10.1021/jp0611018.

[75] A.C.T. van Duin, S. Dasgupta, F. Lorant, W.A. Goddard, ReaxFF: a reactive force field for hydrocarbons, J. Phys. Chem. A 105 (2001) 9396–9409, https://doi.org/10.1021/jp004368u.

[76] G. Broglia, G. Ori, L. Larcher, M. Montorsi, Molecular dynamics simulation of amorphous HfO2 for resistive RAM applications, Model. Simul. Mater. Sci. Eng. 22 (2014) 065006, https://doi.org/10.1088/0965-0393/22/6/065006.

[77] W. Humphrey, A. Dalke, K. Schulten, VMD: visual molecular dynamics, J. Mol. Graph. 14 (33–38) (1996) 27–28.

[78] A. Slassi, F. Tavanti, S. Clima, D. Garbin, A. Calzolari, Schottky contact modulation at a-GeSe/TiN interface for ovonic switching selectors, Appl. Surf. Sci. 689 (2025) 162455, https://doi.org/10.1016/j.apsusc.2025.162455.

[79] W. Scopel, M. Fantini, M. Alayo, I. Pereyra, Local structure and bonds of amorphous silicon oxynitride thin films, Thin Solid Films 413 (2002) 59–64.

[80] M.C. Ridgway, K. Yu, C. Glover, G.J. Foran, C. Clerc, J.L. Hansen, A.N. Larsen, Composition-dependent bond lengths in crystalline and amorphized Ge x Si 1−x alloys, Phys. Rev. B 60 (1999) 10831.

[81] R.V. Meidanshahi, S. Bowden, S.M. Goodnick, Electronic structure and localized states in amorphous Si and hydrogenated amorphous Si, Phys. Chem. Chem. Phys. 21 (2019) 13248–13257.

[82] S. Kyushin, Y. Kurosaki, K. Otsuka, H. Imai, S. Ishida, T. Kyomen, M. Hanaya, H. Matsumoto, Silicon–silicon π single bond, Nat. Commun. 11 (2020) 1–7.

[83] T. Perevalov, V. Gritsenko, S. Erenburg, A. Badalyan, H. Wong, C. Kim, Atomic and electronic structure of amorphous and crystalline hafnium oxide: X-ray photoelectron spectroscopy and density functional calculations, J. Appl. Phys. 101 (2007) 053704.

[84] G. Chen, Z. Hou, X. Gong, Density functional calculations on atomic and electronic structures of amorphous HfO 2/Si (001) interface, Appl. Phys. Lett. 95 (2009) 102905.

[85] A.-M. El-Sayed, M.B. Watkins, T. Grasser, V.V. Afanasev, A.L. Shluger, Hydrogen-induced rupture of strained Si-O bonds in amorphous silicon dioxide, Phys. Rev. Lett. 114 (2015) 115503.

[86] P. Krüger, B. Baumeier, J. Pollmann, First-principles investigation of an epitaxial silicon oxynitride layer on a 6 H-Si C (0001) surface, Phys. Rev. B 77 (2008) 085329.

[87] A.C. Wright, Neutron scattering from vitreous silica. V. the structure of vitreous silica: what have we learned from 60 years of diffraction studies? J. Non-Cryst. Solids 179 (1994) 84–115.

[88] X. Yuan, A. Cormack, Efficient algorithm for primitive ring statistics in topological networks, Comput. Mater. Sci 24 (2002) 343–360.

[89] T.H. Nguyen, V.V. Le, T.N. Nguyen, Molecular dynamics simulation of structural properties in amorphous HfO2 under cooling process, Vacuum 161 (2019) 251–258.

[90] P. Broqvist, A. Pasquarello, First principles investigation of defects at interfaces between silicon and amorphous high-κ oxides, Microelectron. Eng. 84 (2007) 2022–2027.

[91] H.-P. Ma, H.-L. Lu, J.-H. Yang, X.-X. Li, T. Wang, W. Huang, G.-J. Yuan, F. F. Komarov, D.W. Zhang, Measurements of microstructural, chemical, optical, and electrical properties of silicon-oxygen-nitrogen films prepared by plasma-enhanced atomic layer deposition, Nanomaterials 8 (2018), https://doi.org/10.3390/nano8121008.

[92] S. Nekrashevich, V. Gritsenko, Electronic structure of silicon oxynitride: Ab-initio and experimental study, comparison with silicon nitride, J. Appl. Phys. 110 (2011) 114103.

[93] S. Ferrari, S. Spiga, C. Wiemer, M. Fanciulli, A. Dimoulas, Germanium diffusion during HfO2 growth on Ge by molecular beam epitaxy, Appl. Phys. Lett. 89 (2006) 122906, https://doi.org/10.1063/1.2349320.
[94] C. Zechner, N. Zographos, Technology computer-aided design model for SiGe oxidation and Ge diffusion along oxide/SiGe interfaces, Phys. Status Solidi A 221 (2024) 2400235, https://doi.org/10.1002/pssa.202400235.
[95] P. Ganster, A. Saúl, G. Tréglia, Ge condensation under SiGe oxidization: from Molecular Dynamics simulation to one-dimensional analytic modeling, (2012). https://doi.org/10.48550/arXiv.1207.7238.
[96] J.-H. Liao, J.-Y. Hsieh, H.-J. Lin, W.-Y. Tang, C.-L. Chiang, Y.-S. Lo, T.-B. Wu, L.-W. Yang, T. Yang, K.-C. Chen, others, Physical and electrical characteristics of silicon oxynitride films with various refractive indices, J. Phys. Appl. Phys. 42 (2009) 175102.
[97] B. Dianat, F. Tavanti, A. Padovani, L. Larcher, A. Calzolari, BELLO: a post-processing tool for the local-order analysis of disordered systems, Comput. Mater. Sci 209 (2022) 111381, https://doi.org/10.1016/j.commatsci.2022.111381.
[98] F. Tavanti, A. Calzolari, Multi-technique approach to unravel the (dis)order in amorphous materials, ACS Omega 7 (2022) 23255–23264, https://doi.org/10.1021/acsomega.2c01359.